Biochemical and Biophysical Research Communications 557 (2021) 20–25

Contents lists available at ScienceDirect

Biochemical and Biophysical Research Communications

journal homepage: www.elsevier.com/locate/ybbrc

The hydrogen bonding network involved Arg59 in human protoporphyrinogen IX oxidase is essential for enzyme activity

Baifan Wang [1], Zijuan Zhang [1], Hao Zhu, Congwei Niu, Xin Wen*, Zhen Xi**

State Key Laboratory of Elemento-Organic Chemistry and Department of Chemical Biology, National Pesticide Engineering Research Center (Tianjin), Nankai University, 94 Weijin Road, Tianjin, 300071, China

ARTICLE INFO

Article history:
Received 18 March 2021
Accepted 22 March 2021
Available online 12 April 2021

Keywords:
Protoporphyrinogen IX oxidase
Hydrogen bonding network
Enzyme
Molecular dynamics
Mutagenesis

ABSTRACT

Protoporphyrinogen IX oxidase (PPO) is the last common enzyme in chlorophyll and heme biosynthesis pathways. In human, point mutations on PPO are responsible for the dominantly inherited disorder disease, Variegate Porphyria (VP). Of the VP-causing mutation site, the Arg59 is by far the most prevalent VP mutation residue identified. Multiple sequences alignment of PPOs shows that the Arg59 of human PPO (*h*PPO) is not conserved, and experiments have shown that the equivalent residues in PPO from various species are essential for enzymatic activity. In this work, it was proposed that the Arg59 performs its function by forming a hydrogen-bonding (HB) network around it in *h*PPO, and we investigated the role of the HB network via site-directed mutagenesis, enzymatic kinetics and computational studies. We found the integrity of the HB network around Arg59 is important for enzyme activity. The HB network maintains the substrate binding chamber by holding the side chain of Arg59, while it stabilizes the micro-environment of the isoalloxazine ring of FAD, which is favorable for the substrate-FAD interaction. Our result provides a new insight to understanding the relationship between the structure and function for *h*PPO that non-conserved residues can form a conserved element to maintain the function of protein.

1. Introduction

Protoporphyrinogen IX oxidase (PPO, EC 1.3.3.4), a member of superfamily of flavin adenine dinucleotide (FAD)-containing proteins, is the last enzyme in the common tetrapyrrole biosynthesis pathway just before the pathway branches toward chlorophyll and heme synthesis [1–3]. PPO provides protoporphyrin IX (proto IX) for both Mg chelatase and ferrochelatase by catalyzing the oxidation of protoporphyrinogen IX (protogen) (Fig. S1), leading to chlorophyll and heme, respectively [1]. Except for its important biological function [2,4,5], PPO has been a topic of interests in agricultural and medical areas as inhibitor targets [6] and the involvement in human disease [7,8]. Unexpectedly, PPO has been found to be a regulator of plastid RNA editing through interaction with RNA editing factors [9], suggesting that the other functions of PPO remains to be explored.

In humans, point mutations on PPO, resulting in drastically decreased enzymatic activity or in-active enzyme, is responsible for the dominantly inherited disorder disease, Variegate Porphyria (VP) [7,8,10]. VP patients are characterized by an abnormal pattern of porphyrin excretion, and clinical manifestations including photosensitive skin lesions and/or a propensity to develop acute neurovisceral crises [11,12]. To date, over 100 mutations causing VP have been identified (Human Gene Mutation Database, http://www.hgmd.cf.ac.uk/ac/gene.php?gene = PPOX). Of the residues involved in VP causing mutations, the Arg59 is by far the most prevalent VP mutation site identified, more than 94% of the patients in South Africa carrying a Arg59-Trp mutation (R59W) [13,14] which dramatically decrease the activity of human PPO (*h*PPO) *in vitro* [14–17]. However, multiple sequences alignment of PPOs (Fig. 1A) shows that the Arg59 of human PPO (*h*PPO) is not conserved, and the equivalent residues in various species have also been shown to be essential for enzymatic activity and structural stability [18,19].

The residue corresponding to human Arg59 in the mitochondrial tobacco PPO (*mt*PPO) is Asn67. Replacing Asn67 with arginine or tryptophan to mimic the wild-type and R59W mutant of *h*PPO showed that the N67R mutant affected k_{cat} and K_M values of the

* Corresponding author.
** Corresponding author.
E-mail addresses: xinwen@nankai.edu.cn (X. Wen), zhenxi@nankai.edu.cn (Z. Xi).
[1] These authors contribute equally to the work.

https://doi.org/10.1016/j.bbrc.2021.03.124
0006-291X/

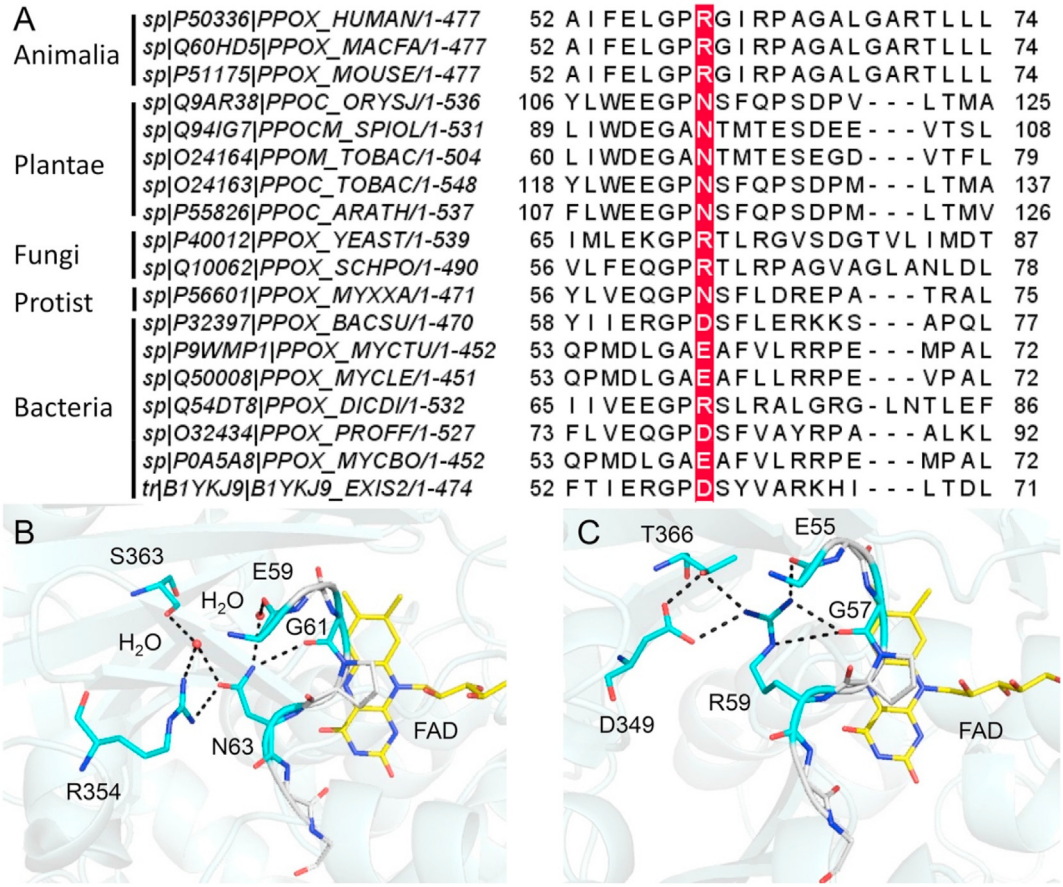

Fig. 1. A: Sequence alignment of PPO from various species. The residues corresponding to Arg59 of *h*PPO is labeled. The HB network surrounding Asn63 in *mx*PPO (B) and Arg59 in *h*PPO (C). H-bonds are showing in dash.

*mt*PPO, while the N67W abolished enzyme activity, indicating an important role of Asn67 in the *mt*PPO.

In the crystal structure of *Myxococcus xanthus* PPO (*mx*PPO), the Asn63 (equivalent to Arg59 of *h*PPO) is surrounding by a hydrogen-bonding (HB) network (Fig. 1B) [18]. Asn63 forms hydrogen bonds (H-bonds) with Arg354, plus water mediated H-bonds with Ser363, Glu59, and the N5 and O4 atoms of cofactor FAD (Fig. 1B). Based on these features, Corradi et al. proposed that this HB network is important for the integrity and stability of PPO active site, holding together the FAD and the substrate-binding domains [18]. However the role of this HB network remains to be explored.

In the *h*PPO structure, we found that Arg59 is also involved in a HB network, in which Arg59 makes H-bonds with the side chains of Asp349 and Thr366, as well as the backbone carbonyl oxygen atoms of Glu55 and Gly57 (Fig. 1C). It is noteworthy that the Asp349 also is a proven pathogenic mutation site involved in VP [17,20,21], and this residue is also not conserved. Furthermore, our structural study on *h*PPO R59G and R59Q mutants (Fig. S2) also showed that Arg59 is response for the stability of loop comprise of Leu56-Ile61, which might be required for the properly binding of the isoalloxazine ring of FAD and the substrate [17].

The hypothesis about the role of this HB network provides a new insight to understanding the relationship between the structure and function of PPO. However, until now no direct experimental evidence has been presented in support of this hypothesis. Thus, in this work we investigated the HB network involved Glu55, Gly57 Arg59, Asp349 and Thr366 in *h*PPO by performed site-directed mutagenesis, enzymatic kinetics and computational studies, which should help to pinpoint functionally important parts and enzymatic action of *h*PPO.

2. Materials and methods

2.1. Expression and purification of the wild-type hPPO and its mutants

Mutations of *h*PPO were generated from the recombinant plasmid (pHPPO-X) using DpnI mediated site-directed mutagenesis methods and confirmed by DNA sequencing. The wild-type *h*PPO and its mutants were expressed and purified as described previously [16]. Briefly, the recombinant proteins were expressed in BL21(DE3)pLysS E.coli cells by induction with 1 mM IPTG at 25 °C for 4 h. Cells were harvested and lysed by sonication. The His-tagged proteins were purified by Ni^{2+}-NTA affinity chromatography. Protein concentration was determined using Bradford method (Bio-Rad).

2.2. Enzymatic assay for kinetic analysis

PPO activity was assayed by measuring the constant velocity of formation of proto IX from protogen using the continuous fluorometric methods at 25 °C by measuring the product which has a maximum excitation wavelength at 410 nm and a maximum emission wavelength at 630 nm. The total volume of the reaction mixture was 200 μL consisting of 0.1 M potassium phosphate buffer (pH 7.4), 5 μM FAD, 5 mM DTT, 1 mM EDTA, 0.2 M imidazole, and

0.03% Tween 80 (*v*/*v*). The enzymatic reaction started by the addition of substrate. The autoxidation rates were determined concomitantly and were subsequently subtracted. Kinetic parameters including the Michaelis–Menten constant (K_M), the maximal velocity (V_{max}) and the catalytic constant (k_{cat}) were determined by the least-squares fitting of the data to the equation using the nonlinear regression method with the following equation:

$$v = \frac{V_{max}[S]}{K_M + S}$$

2.3. Molecular dynamics simulation

Molecular dynamics (MD) simulations for *h*PPO wild-type and mutants listed in Table 1 in complexed with or without protogen (labeled with the SUB and APO, respectively) were carried out. The crystal structure of the wild-type *h*PPO (PDB ID: 3NKS [16]) was used as the starting point for MD simulations. The structures of *h*PPO mutants were generated from the wild-type structure by the mutation of corresponding residues using InsightII (Accelrys Inc., San Diego, CA, USA) as previous studies [17]. The coordinates of protogen and force field parameters of FAD and protogen were taken from previous studies [16,17].

Each of the protein (complex) was immersed in a truncated octahedral box of TIP3P water molecules with the border at least 8 Å away from solutes. The charges of each system were neutralized by adding counter ions (Cl^- or Na^+). MD simulations were carried out with the SANDER module of AMBER 9 [22]. Prior to MD simulations, the studied systems were subjected to three stages of energy minimizations with 500 kcal/mol^{-1}•Å^{-2} restraint on the solutes, with restraint on the non-hydrogen atoms of the solutes and no restraint applied, respectively.

The systems were heated from 0 to 300 K for 50 ps with position restraints of 2 kcal mol^{-1} Å^{-2} on the solute. Equilibrating calculation was executed at 1 atm and at 300 K for 50 ps with 2 kcal/mol^{-1}•Å^{-2} restraint on the solute. Periodic boundary conditions were used, and electrostatic interactions were calculated by the particle mesh Ewald method [23], with the non-bonded cutoff set to 8 Å. The SHAKE method [24] was applied to bonds involving hydrogen, and a 2 fs integration step was used. Pressure was held constant at 1 atm with relaxation time of 2.0. The temperature was held at 300 K with Langevin dynamics [25] with a collision frequency of 2.0. The snapshot of the system was taken for every 1 ps. Production runs of 5 ns without any restraints were carried out.

The ptraj module in the AMBER 9 was used to analyze the MD trajectories. Trajectories after the initial 2 ns of equilibration were considered for analysis. The H-bond occupancy is defined as the percentage of simulation time during which the H-bond donor (D) and the acceptor (A) distance is less than 3.5 Å and the angle (A … H-D) is larger than 120.0°. Average conformation for each simulation was calculated and was subjected to a short minimization of 100 steps by SANDER.

2.4. Calculation of the probability of privileged conformations

The detailed procedure for calculating the probability of privileged conformations (PC) was described in the previous study [17]. Briefly, a set of parameters to describe the conformational space of a studied system should be designated first. Here the distance between C5 atom of protogen and N5 atom of FAD ($D_{C5\text{-}N5}$) and the angle between C5, N5 and N10 ($A_{C5\text{-}N5\text{-}N10}$) (shown in Fig. S3) as geometry parameters were used to describe the reactant conformational space [17]. The MD trajectory between 2 ns and 5 ns yielded 3000 conformations for each studied system was considered for analysis. Thus, 3000 sets of $D_{C5\text{-}N5}$-$A_{C5\text{-}N5\text{-}N10}$ were obtained for each studied system. Then the sets of discrete data points of $D_{C5\text{-}N5}$-$A_{C5\text{-}N5\text{-}N10}$ pairs were converted to the conformation probability density function (CPDF).

Based on the statistical study on the X-ray structures of the flavoenzymes complexes with substrate or substrate analogues [26], we defined the conformations with $D_{C5\text{-}N5}$ within 3.0–3.8 Å and $A_{C5\text{-}N5\text{-}N10}$ within 96–117° as the privileged conformations of *h*PPO. For each studied system, the probability of PC, denoted P_{PC}, was calculated by the bivariate integration of corresponding CPDF over the interval [96, 117] for $A_{C5\text{-}N5\text{-}N10}$, and [3.0, 3.8] for $D_{C5\text{-}N5}$ using Matlab software (The Math Works, Natick, MA). The activity for each mutants were predicted by the following function [17] and was transformed to the relative k_{cat}/K_M values.

$$k_{cat} \Big/ K_M = 0.11(e^{4.84*P}PC - 1)$$

3. Results and discussion

3.1. The integrity of the HB network around Arg59 is important for enzyme activity

To explore the role of the HB network around Arg59 in *h*PPO, we constructed a series of mutants by the replacement of Arg59 and Asp349 with conserved and non-conserved residues (Table 1). The kinetic study of these mutants showed that the conserved mutation of Arg59 (R59K) and Asp349 (D349E) can maintain about 80% of the wild-type activity, while the non-conserved mutations resulted in less than 50% of the wild-type activity. The side chain of Thr366 is also involved in the formation of the HB network, and the T366A mutant reduced to about 65% of the wild-type activity (Table 1).

Table 1
Enzymatic Kinetic and H-bond occupancy of wild-type *h*PPO and its mutants.

Enzyme	K_M (μM)	k_{cat} (min^{-1})	k_{cat}/K_M (min^{-1}μM^{-1})	Relative activity	H-bond occupancy (%)[a]	P_{PC}[c]	Relative activity (predicted)[d]
Wild type	1.405	11.501	8.186	100.00%	482 (355)[b]	0.65	93.03%
R59K	1.865	12.589	6.750	82.46%	298 (257)	0.61	81.44%
R59A	1.162	4.198	3.613	44.13%	0 (0)	0.59	73.51%
R59E	2.980	5.542	1.860	22.72%	0 (0)	0.29	13.77%
D349E	1.253	8.696	6.940	84.78%	432 (355)	0.59	73.51%
D349A	2.080	1.371	0.659	8.05%	94 (0)	0.23	9.17%
D349R	3.580	0.728	0.203	2.48%	0 (0)	0.06	1.51%
T366A	1.768	9.328	5.276	64.45%	324 (375)	0.50	45.97%

[a] The sum of the occupancy of all of the H-bonds in network.
[b] Number in parenthesis are the values for H-bond occupancy in SUB simulation.
[c] The probabilities of the privileged conformation.
[d] Relative activity values predicted from P_{PC} values.

The structures of the wild-type *h*PPO and its mutants listed in Table 1 as well as their complex with protogen were constructed and subjected to MD simulation. We examined the situation of the HB network around Arg59 by calculating the H-bond occupancy for each of the studied systems during simulations. All of the H-bonds in the HB network were well maintained in the simulation of wild-type *h*PPO (Fig. 2, Tables 1 and S1). The R59K mutant lost the H-bond between Arg59 and Gly57 while the other H-bonds were stable. In the D349E mutant only the H-bond between Arg59 and Thr366 was weaken relative to the one in the wild-type *h*PPO. The T366A mutation caused the loss of the H-bonds between Arg59 and Gly57, Arg59 and Thr366, as well as the weakening of the H-bond between Arg59 and Glu55, and the enhancement of the H-bond interactions between Arg59 and Asp349. For the rest of mutants, only the D349A can hold the H-bond between Arg59 and Gly57, but most of the H-bond interactions were lost. It was found that there is a positive correlation between the H-bond occupancies with the activities of wild-type *h*PPO and its mutants. These results indicated that the integrity of the HB network around Arg59 is important for the activity of *h*PPO and its mutants.

3.2. The HB network maintains the substrate binding chamber

Arg59 residue has a long and flexible side chain. The side chain was well held by the HB network in the wild-type *h*PPO during APO simulation (Fig. 1 and 2), while for the *h*PPO mutants, once the H-bonds between 59th residue and the related residues were missing, the 59th residues with a long side chain would display large movements. From APO simulation it can be found that the side chain of 59th residue invaded the active site of R59E, D349A and D349R mutant, respectively and even was close to the floor of the active site (Fig. 2). The minimum distance between 59th residues and Gly169 which is protruding from the floor of the active site ($D_{59\text{-}G169}$, Fig. S4) was calculated to characterize the movement of the 59th residues in the active site during APO simulations. Table S2 and Fig. S4 showed the distribution of $D_{59\text{-}G169}$ versus the relative activity of the studied systems. It is interesting to found that, for the mutants with higher activity (>60%), as well as with lower H-bond occupancy, the values of the $D_{59\text{-}G169}$ correspond to maxima distribution are more than 9.0 Å; while for the other mutants, the ones are less than 9.0 Å. Thus, for R59E, D349A and D349R mutants, the structure of their active site was abolished by the preoccupation of the side chain of Arg59 or Asp59, which should inferior the binding of the substrate and were supported by the larger K_M values of these mutants.

We also investigated the potential close contacts between substrate and the side chain of 59th residue in the wild-type *h*PPO and its mutants during the SUB simulations, showing the average conformations for each studied system in Fig. S5. We evaluated the contacts between the 59th residues and protogen by the minimum distances between the non-hydrogen atoms of 59th residues and protogen. We defined that once the distance is smaller than 5.0 Å, there is a close contact among the 59th residue and protogen. Table S2 indicates that the side chain of 59th residue in R59E, D349A and D349R mutants made intensive close contacts with protogen, while there were not close contacts between the 59th residues and protogen in the wild-type, R59K, R59A, D349E and T366A mutants. Such close contacts should be unfavor for the performance of the enzymatic function since it may disturb binding and orientation of protogen within the active site of mutants. Considering the H-bond occupancy for studied systems, it is reasonable to infer that the HB network could maintain the integrity of substrate binding chamber.

3.3. The HB network is essential for the stability of the loop above the isoalloxazine ring of FAD

Arg59 is located in a loop structure (residues 56–61) above the isoalloxazine ring of FAD. In this loop residue Pro58 forms a van der Waals interaction with the isoalloxazine of FAD (Fig. 3), and the mutation of the residue Gly57 to Arg has been found to cause VP disease [27], indicating an important role of this loop. We examined the conformational dynamics of this loop from MD simulation for each of the studied systems. It is indicated that the loop in mutants display a definite shift relative to the one in the wild-type (Fig. 3). We calculated the RMSD value of the loop for each of the mutants using the average conformation of wild-type *h*PPO as the reference structure. It could be seen from Table S2 that the loops in the mutants D349E, R59K and T366A demonstrated stability since the lower values of RMSD were observed in these systems, while other mutants showed the RMSD values larger than 0.5, indicating that in these mutants, the loop structures underwent large movement and structural change relative to the one in the wild-type *h*PPO.

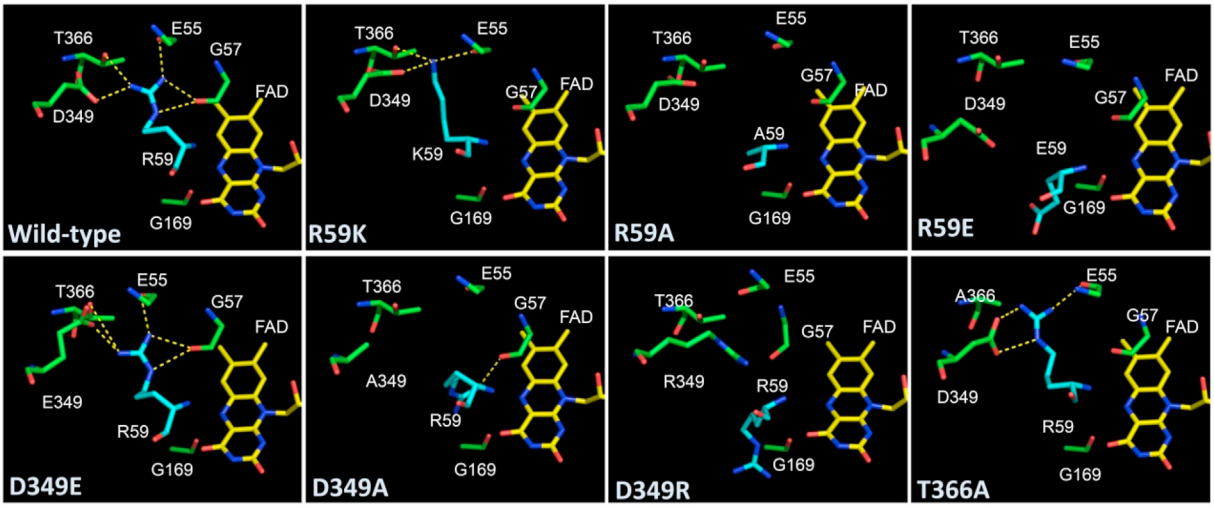

Fig. 2. Averaged conformations for the 59th residues of the studied systems form APO simulations. The residues in the HB network as well as an "anchor residue" Gly169 are shown, the sidechain of Glu55 are not shown for clarity.

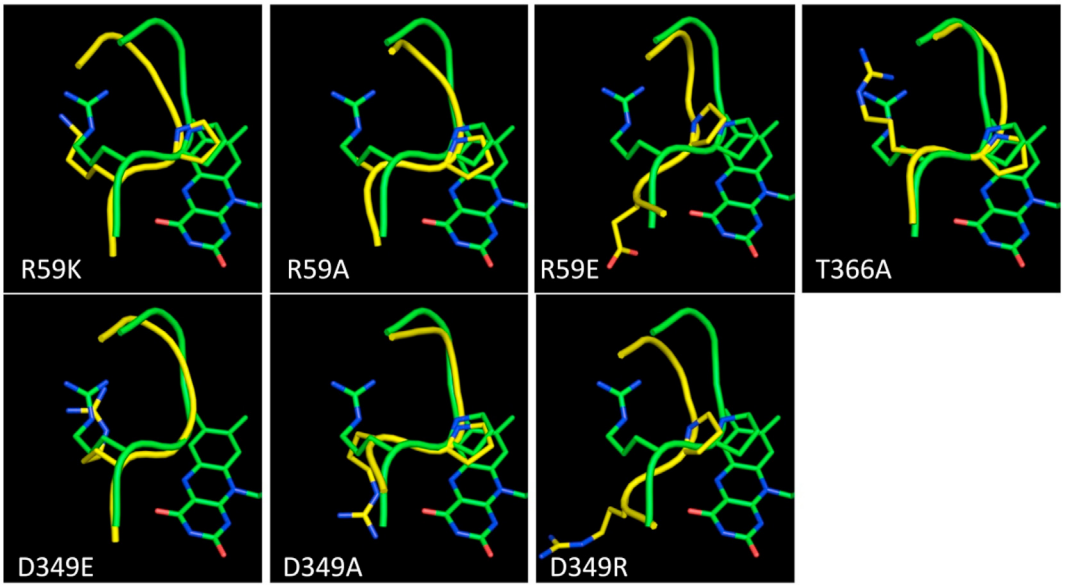

Fig. 3. Comparison of the loop structure formed by residues 56–61 in the SUB simulation. The structures from mutants were aligned to the wild-type by fit the isoalloxazine ring of FAD. The wild-type is shown in green, while the mutants are shown in yellow. (For interpretation of the references to colour in this figure legend, the reader is referred to the Web version of this article.)

By compared to the H-bond occupancy, it was clear that the H-bonds could steady the loop by restrained the 59th residues, while the loss of the restriction for the 59th residue could affect the local environment of the isoalloxazine ring of FAD since the loop lies above the isoalloxazine ring of FAD. Thus, an integrated HB network should be essential for the stability of the isoalloxazine ring of FAD.

3.4. The HB network affects the conformational distribution of the reactants

In our previous study, we found the conformational distribution of the reactants (protogen and FAD) in the equilibrium systems could be used as an indicator for the activity of *h*PPO [17]. We defined the conformations within a reactable range as the privileged conformation (PC), and the probabilities of PC (P_{PC}) can correlated with the activities of wild-type *h*PPO and a series of its mutants. In this study, the P_{PC} for each studied systems were calculated (listed in Table 1, S3 and S4). We observed a nice correlation between the P_{PC} and the activity of wild-type and mutants, and the uniformity between the activities with the integrity of the HB network around Arg59. These indicated that the HB network should affect the ability of the sampling conformations which are suitable for the catalysis in *h*PPO and its mutants.

In conclusion, the role of the HB network in *h*PPO should be to keep the long side chain of Arg59 to prevent unfavored contacts with substrate, while stabilize the micro-environment of the isoalloxazine ring of FAD, which is favorable for the protogen-FAD interaction. Taken together, the HB network should help to the formation of privileged conformations of the reactants (protogen and FAD), thereby maintaining the activity of *h*PPO.

We note that similar HB network is also present in other species of PPO (Figs. 1 and S6). These HB networks are composed of either direct H-bonds formed between residues or water-mediated H-bonds. For example, in *mt*PPO, the side chain of residue Asn67 (corresponding to Arg59 in *h*PPO) makes H-bonds with the backbone Gly65 and Asp63, plus water-mediated H-bond with Thr390 and Ser374 (corresponding to Thr356 and Asp349 in *h*PPO, respectively.) Previous study using the double mutation of N67R/S374D in *mt*PPO with the aim to mimic the residue pair of Arg59-Asp349 in *h*PPO, resulted in an increase of the activity of PPO to about 3.6 fold of the wild-type *mt*PPO [19]. This result thus implicated an import role of the HB network in *mt*PPO.

Although the residues corresponding to Arg59 of *h*PPO are not conserved in various species, they might share common feature: their side chains are polar, such as arginine, aspartic acids and glutamic acid, which make them able to form more than one H-bond. A cluster of amino acids, such as the HB network, with a particular property might play a significant role relative to the overall composition of the protein. Identification of such residue network in known protein structure may help to pinpoint functionally important parts of protein structure.

Declaration of competing interest

None declared.

Acknowledgements

This study was supported by the National Natural Science Foundation of China (21672118) and the National Key Research and Development Program of China (No. 2017YFD0200500). We are grateful to Shanghai Supercomputer Center of China and National Supercomputing Center in Tianjin for providing computational resources.

Appendix A. Supplementary data

Supplementary data to this article can be found online at https://doi.org/10.1016/j.bbrc.2021.03.124.

References

[1] R. Poulson, The enzymic conversion of protoporphyrinogen IX to protoporphyrin IX in mammalian mitochondria, J. Biol. Chem. 251 (1976) 3730–3733.
[2] G. Layer, J. Reichelt, D. Jahn, D.W. Heinz, Structure and function of enzymes in heme biosynthesis, Protein Sci. 19 (2010) 1137–1161.
[3] H.A. Dailey, T.A. Dailey, S. Gerdes, D. Jahn, M. Jahn, M.R. O'Brian, M.J. Warren, Prokaryotic heme biosynthesis: multiple pathways to a common essential

product, Microbiol. Mol. Biol. Rev. 81 (2017) e00016–e48.
[4] H.A. Dailey, Biosynthesis of Heme and Chlorophylls, McGraw-Hill, New York, 1990.
[5] P. Brzezowski, B. Ksas, M. Havaux, B. Grimm, M. Chazaux, G. Peltier, X. Johnson, J. Alric, The function of PROTOPORPHYRINOGEN IX OXIDASE in chlorophyll biosynthesis requires oxidised plastoquinone in Chlamydomonas reinhardtii, Commun. Biol. 2 (2019) 1–9.
[6] S.O. Duke, J. Lydon, J.M. Becerril, T.D. Sherman, L.P. Lehnen Jr., H. Matsumoto, Protoporphyrinogen oxidase-inhibiting herbicides, Weed Sci. (1991) 465–473.
[7] J.C. Deybach, H. de Verneuil, Y. Nordmann, The inherited enzymatic defect in porphyria variegata, Hum. Genet. 58 (1981) 425–428.
[8] P.N. Meissner, A.V. Corrigall, R.J. Hift, Fifty years of porphyria at the university of cape town, S, Afr. Med. J. 102 (2012) 422–426.
[9] F. Zhang, W.J. Tang, B. Hedtke, L.L. Zhong, L. Liu, L.W. Peng, C.M. Lu, B. Grimm, R.C. Lin, Tetrapyrrole biosynthetic enzyme protoporphyrinogen IX oxidase 1 is required for plastid RNA editing, Proc. Natl. Acad. Sci. U.S.A. 111 (2014) 2023–2028.
[10] P.N. Meissner, R.S. Day, M.R. Moore, P.B. Disler, E. Harley, Protoporphyrinogen oxidase and porphobilinogen deaminase in variegate porphyria, Eur. J. Clin. Invest. 16 (1986) 257–261.
[11] G.H. Elder, R.J. Hift, P.N. Meissner, The acute porphyrias, Lancet (N. Am. Ed.) 349 (1997) 1613–1617.
[12] H. Puy, L. Gouya, J.-C. Deybach, Porphyrias, Lancet 375 (2010) 924–937.
[13] L. Warnich, M.J. Kotze, I.M. Groenewald, J.Z. Groenewald, M.G. Van Brakel, C.J. Van Heerden, J.N.P. De Villiers, W.J.M. Van De Ven, E.F.P.M. Schoenmakers, S. Taketani, A.E. Retief, Identification of three mutations and associated haplotypes in the protoporphyrinogen oxidase gene in South African families with variegate porphyria, Hum. Mol. Genet. 5 (1996) 981–984.
[14] P.N. Meissner, T.A. Dailey, R.J. Hift, M. Ziman, A.V. Corrigall, A.G. Roberts, D.M. Meissner, R.E. Kirsch, H.A. Dailey, A R59W mutation in human protoporphyrinogen oxidase results in decreased enzyme activity and is prevalent in South Africans with variegate porphyria, Nat. Genet. 13 (1996) 95–97.
[15] M.H. Maneli, A.V. Corrigall, H.H. Klump, L.M. Davids, R.E. Kirsch, P.N. Meissner, Kinetic and physical characterisation of recombinant wild-type and mutant human protoporphyrinogen oxidases, Biochim. Biophys. Acta Protein Proteonomics 1650 (2003) 10–21.
[16] X. Qin, Y. Tan, L. Wang, Z. Wang, B. Wang, X. Wen, G. Yang, Z. Xi, Y. Shen, Structural insight into human variegate porphyria disease, Faseb. J. 25 (2011) 653–664.
[17] B. Wang, X. Wen, X. Qin, Z. Wang, Y. Tan, Y. Shen, Z. Xi, Quantitative structural insight into human variegate porphyria disease, J. Biol. Chem. 288 (2013) 11731–11740.
[18] H.R. Corradi, A.V. Corrigall, E. Boix, C.G. Mohan, E.D. Sturrock, P.N. Meissner, K.R. Acharya, Crystal structure of protoporphyrinogen oxidase from Myxococcus xanthus and its complex with the inhibitor acifluorfen, J. Biol. Chem. 281 (2006) 38625–38633.
[19] I. Heinemann, N. Diekmann, A. Masoumi, M. Koch, A. Messerschmidt, M. Jahn, D. Jahn, Functional definition of the tobacco protoporphyrinogen IX oxidase substrate-binding site, Biochem. J. 402 (2007) 575–580.
[20] A.G. Roberts, H. Puy, T.A. Dailey, R.R. Morgan, S.D. Whatley, H.A. Dailey, P. Martasek, Y. Nordmann, J.-C. Deybach, G.H. Elder, Molecular characterization of homozygous variegate porphyria, Hum. Mol. Genet. 7 (1998) 1921–1925.
[21] X. Qin, L. Sun, X. Wen, X. Yang, Y. Tan, H. Jin, Q. Cao, W. Zhou, Z. Xi, Y. Shen, Structural insight into unique properties of protoporphyrinogen oxidase from Bacillus subtilis, J. Struct. Biol. 170 (2010) 76–82.
[22] J.M. Wang, W. Wang, P.A. Kollman, D.A. Case, Automatic atom type and bond type perception in molecular mechanical calculations, J. Mol. Graph. Model. 25 (2006) 247–260.
[23] T. Darden, D. York, L. Pedersen, Particle mesh Ewald - an N.log(N) method for Ewald sums in large systems, J. Chem. Phys. 98 (1993) 10089–10092.
[24] J.P. Ryckaert, G. Ciccotti, H.J.C. Berendsen, Numerical-integration of cartesian equations of motion of a system with constraints - molecular-dynamics of N-alkanes, J. Comput. Phys. 23 (1977) 327–341.
[25] H.J.C. Berendsen, J.P.M. Postma, W.F. Vangunsteren, A. Dinola, J.R. Haak, Molecular-dynamics with coupling to an external bath, J. Chem. Phys. 81 (1984) 3684–3690.
[26] M.W. Fraaije, A. Mattevi, Flavoenzymes: diverse catalysts with recurrent features, Trends Biochem. Sci. 25 (2000) 126–132.
[27] V. Pinder, S. Holden, C. Deshpande, A. Siddiqui, J. Mellerio, E. Wraige, A. Powell, Homozygous variegate porphyria presenting with developmental and language delay in childhood, Clin. Exp. Dermatol. 38 (2013) 737–740.